Molecular Crystals and Liquid Crystals Science and Technology. Section A. Molecular Crystals and Liquid Crystals

Publication details, including instructions for authors and subscription information:
http://www.tandfonline.com/loi/gmcl19

DNA Mesophases: A Structural Analysis in Polarizing and Electron Microscopy

Françoise Livolant [a] & Amélie Leforestier [a]

[a] Centre de Biologie Cellulaire (CNRS), 67, rue Maurice Günsbourg, 94200, Ivry-sur-Seine, (FRANCE)

Version of record first published: 24 Sep 2006.

To cite this article: Françoise Livolant & Amélie Leforestier (1992): DNA Mesophases: A Structural Analysis in Polarizing and Electron Microscopy, Molecular Crystals and Liquid Crystals Science and Technology. Section A. Molecular Crystals and Liquid Crystals, 215:1, 47-56

To link to this article: http://dx.doi.org/10.1080/10587259208038510

Mol. Cryst. Liq. Cryst. 1992, Vol. 215, pp. 47–56
Reprints available directly from the publisher
Photocopying permitted by license only

Printed in the United States of America

DNA MESOPHASES
A STRUCTURAL ANALYSIS IN POLARIZING AND ELECTRON MICROSCOPY

Françoise LIVOLANT, Amélie LEFORESTIER
Centre de Biologie Cellulaire (CNRS), 67, rue Maurice Günsbourg,
94200 Ivry-sur-Seine (FRANCE)

(*Received April 5, 1991*)

Abstract

In aqueous solution, pure DNA forms multiple liquid crystalline phases when the polymer concentration is increased. A structural analysis of the different phases and of their transitions is presented here in polarizing and in electron microscopy.The cholesteric phase presents usually periodic patterns with series of nested arches in electron microscopy. The defects of the structure can be analyzed with the resolution of the electron microscopy and compared to the data available in polarizing microscopy. We show how the germs of the more concentrated phase nucleate preferentially along some types of defects of the cholesteric phase. The concentrated phase is columnar hexagonal and behaves as a lamellar structure. Each layer (25 to 40 Å thick) is composed of DNA molecules aligned in parallel. Numerous screw dislocations, either left or right-handed, can be seen in the structure. Besides, the evolution of the hexagonal textures, induced by a progressive dehydration of the preparation, can be followed with the resolution of the electron microscopy. Finally, the biological interest of the liquid crystalline structure of DNA is discussed.

Keywords: DNA, mesophases, structure, microscopy

INTRODUCTION

In the cells, the DNA molecule is extremely long and associated with proteins to form chromatin which can be extremely compacted in chromosomes, sperm nuclei and virus capsids. The local DNA concentration can reach values up to 800 mg/ml as estimated by Kellenberger [1]. Pure DNA forms *in vitro* liquid crystalline phases in the same range of concentration [2-13]. We investigate the structure of these liquid crystalline phases in polarizing and electron microscopy in order to compare these phases with the condensed forms of chromatin *in vivo*.

MATERIAL AND METHODS

DNA fragments of about 50nm were prepared by selective digestion of calf thymus chromatin according to the procedure described in [13]. The concentrated solutions of DNA (> 200 mg/ml) were prepared in saline buffers (0.25 M ammonium acetate or 0.25 M

sodium chloride, pH 7).

Microscopy : A drop of the liquid crystalline solution was deposited between slide and coverslip and observed in a Nikon Optiphot X Pol microscope, between crossed linear or circular polars. For cryoelectron microscopy, samples were placed onto copper discs. Different cryofixation methods have been compared [14]. Two of them were used in these experiments. In the first one (used for the cholesteric phase), the samples were projected onto a copper block cooled down to -269°C with a velocity of about 3 $m.s^{-1}$ in a Reichert-Jung cryovacublock. They were immediately transferred and stored in liquid nitrogen. In the second method (used for the hexagonal phase), 10 to 30% (v/v) glycerol (cryoprotectant) was added to the DNA solution without any visible modification of the textures in polarizing microscopy. The samples were quickly frozen by immersion in liquid freon 22 (-160°) cooled in liquid nitrogen, and immediately transferred in liquid nitrogen. Samples were fractured at -110°C under a 2.10^{-7} Torr vacuum. The surface of the sample was unidirectionally shadowed with platinum/carbon at an angle of 45° and carbon coated. After being washed in distilled water, the replicas were observed in a 201 Philips transmission electron microscope.

RESULTS

In aqueous solution, DNA forms different liquid crystalline phases and their nature depends on the polymer concentration as described in Fig. 1.

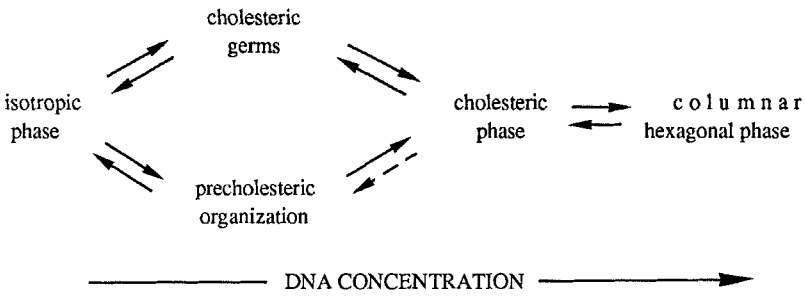

FIGURE 1 : Multiple liquid crystalline phases of DNA

When the DNA concentration is increased, the isotropic phase turns to cholesteric[2,3,6,7,9], and then to columnar hexagonal [8,12]. There are two transitions between the isotropic and the cholesteric phase. In the first one, germs of the cholesteric phase grow in the isotropic phase and merge to form the cholesteric phase [6].In the second one, that we call precholesteric, the transition seems to be continuous between the isotropic and the cholesteric phase, with a complex helical organization of molecular

orientations [15]. This organization seems to be specific of long DNA fragments. In this article, we will focuse our attention on the cholesteric and hexagonal phases.

Cholesteric phase

The cholesteric phase often presents classical fingerprint patterns in polarizing microscopy, as shown in Fig. 2a. The helical pitch P usually ranges from 2 to 3 μm and does not seem to depend on the concentration of DNA and ions in the solution[16]. However, we measured smaller (0.2 to 0.4 μm) or larger pitches (> 5 μm) when the cholesteric phase is close to the transition to the more concentrated phase. This cholesteric periodicity is easily recognizable in electron microscopy, at low magnification (Fig. 2b). Reliefs superimpose to this layering pattern. They are formed during the fracture process and they present the same periodicity as the cholesteric structure itself. At higher magnification, the layers appear very often as series of nested arches. These patterns originate from the cholesteric structure itself, when the fracture plane is oblique with respect to the cholesteric stratification, as explained in Fig. 3. Other orientations of the fracture plane relative to the cholesteric structure lead to other patterns : periodic patterns without arches when the fracture plane is parallel to the cholesteric axis (Fig 3b) or a parallel alignment of molecules when the fracture plane is normal to the cholesteric axis (Fig. 3d) [17]. These patterns are less frequent and they are not illustrated here.

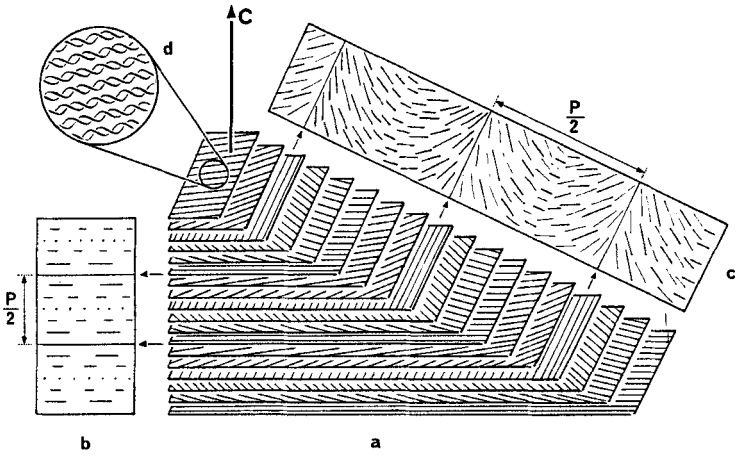

FIGURE 3 Schematic drawing of the cholesteric structure with its different possible patterns in electron microscopy. The DNA double helices (**d**) are aligned in parallel. Their orientation rotates from one plane to the next. Oblique fracture planes give rise to rows of nested arches (**c**) created by the projection of the different molecular orientations onto the fracture plane. The periodicity corresponds to half the helical pitch (P/2). Fracture planes parallel to the cholesteric axis (C) lead to periodic patterns without arches (**b**) and a parallel alignment of molecules is observed when the fracture plane is normal to the cholesteric axis (**d**).

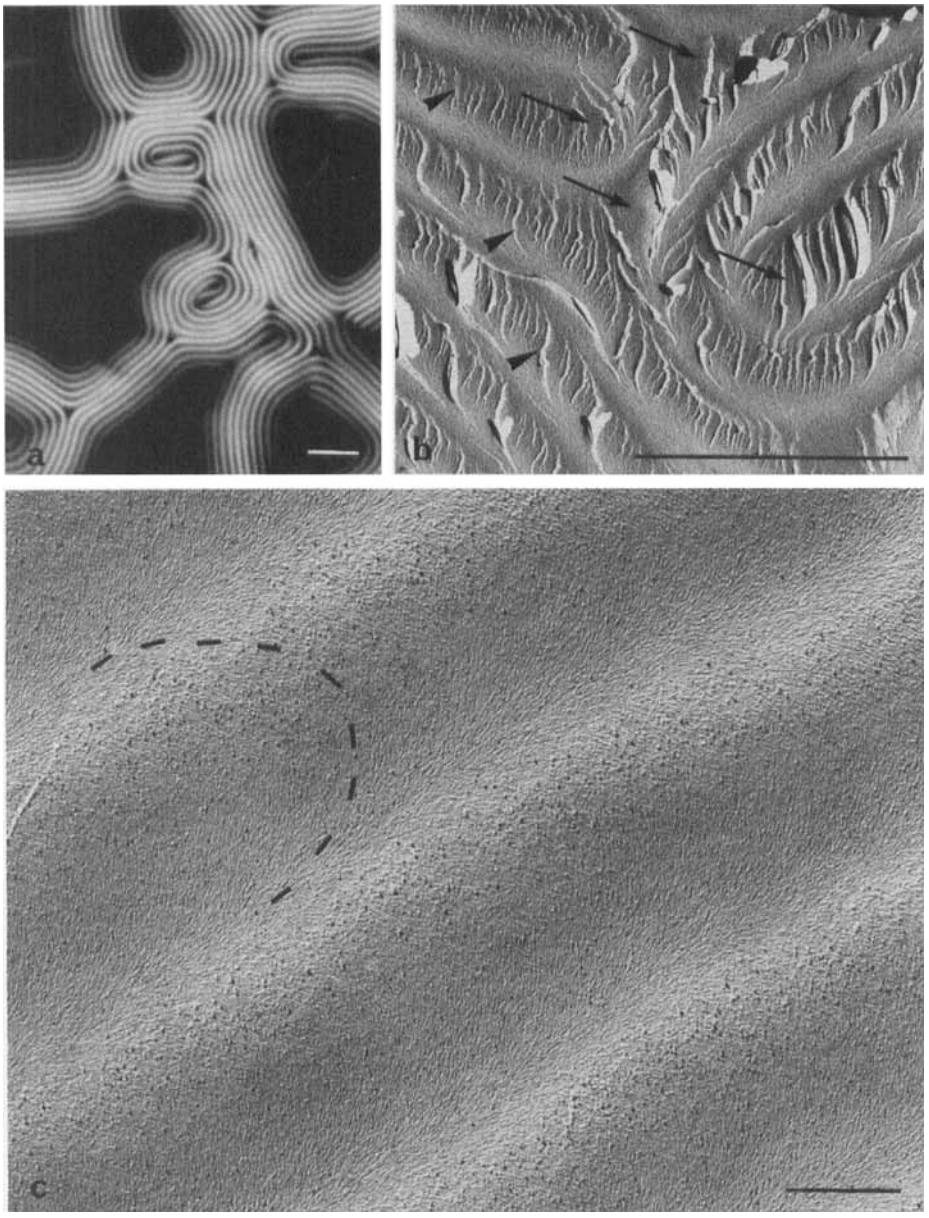

FIGURE 2 Cholesteric phase of DNA. **a** : Classical fingerprint patterns observed in polarizing microscopy (bar = 10 μm). **b** : Freeze-fracture replica observed at low magnification. The cholesteric stratification and its defects (⟶) can be easily recognized (bar = 5 μm). Fracture reliefs (►) superimpose to this pattern. **c** : Higher magnification of the cholesteric stratification permits us to follow accurately the molecular orientations. The arched patterns arise from fractures oblique with respect to the cholesteric axis (bar = 1 μm).

The different defects of this phase, already analyzed in polarizing microscopy [7] are recognized in electron microscopy. The precise orientations of molecules can be analyzed in the core of the defects. We observed + π and - π disclinations and numerous dislocations (Leforestier and Livolant, in preparation).

Transition between the cholesteric and the hexagonal phase

When the DNA concentration is increased, the cholesteric phase transforms into a columnar hexagonal phase [12]. This transition, monitored by NMR methods [18], can be followed in polarizing and in electron microscopy. It turns out that different phase transitions can occur (work in progress). In one of them, the germs of the columnar phase can be seen growing in the cholesteric phase (Fig. 4).The presence of the smallest germs (less than 0.2 μm) can be detected in electron microscopy (Fig 4b). 25% of them are observed in the close vicinity of defect lines (Fig. 4c). It is well known that the defects are involved in phase transition processes. It appears that some of them are more favourable sites for the nucleation of these germs : defects are localized in the core of dislocation lines ($\tau^-\lambda^+$ or $\lambda^-\tau^+$), which corresponds to the addition of 1 or 3 cholesteric layers in the structure (Burger's vector = P/2 or 3P/2). At the transition, all these defects present a germ whereas we never observed hexagonal germs along the other types of dislocation lines or along disclination lines, either +π or -π (in preparation).

Columnar hexagonal phase

We showed previously that the concentrated phase is columnar hexagonal whether it is made of long molecules (0.05 μm to 1.9 μm) [8] or of 500 Å DNA fragments [12]. The DNA molecules are unidirectionnally aligned and form a hexagonal network in section (Fig. 5b). This structure can be considered as a lamellar structure, each layer (about 25 to 40 Å) being made of DNA molecules aligned in parallel [19]. There are therefore three series of layers (1,2,3) corresponding to the three main directions of the hexagonal network. During the freeze-fracture experiments, the fracture plane follows preferentially these molecular layers (Fig. 5a). The molecules themselves can be seen individually at the limit of each plane. They are all aligned parallel to one direction n. This method permits us to detect the presence of numerous defects in the structure, namely screw dislocations [19]. When the fracture plane is oblique with respect to the layers of molecules, the fracture occurs by steps from one layer of molecules to the next one, giving rise to more or less regular striated patterns as illustrated in Fig. 6b,d.

The evolution of the textures induced by a slow evaporation of the solvent was followed in polarizing and in electron microscopy. The fan-shaped textures are first very supple. As determined by a quartz first order retardation plate in polarizing microscopy, the molecular orientation rotates continuously around +π disclination lines (Fig. 6a). This curvature of the molecular layers can be seen in electron microscopy (Fig. 6b). When the polymer concentration increases, the supple domains transform into striated domains as

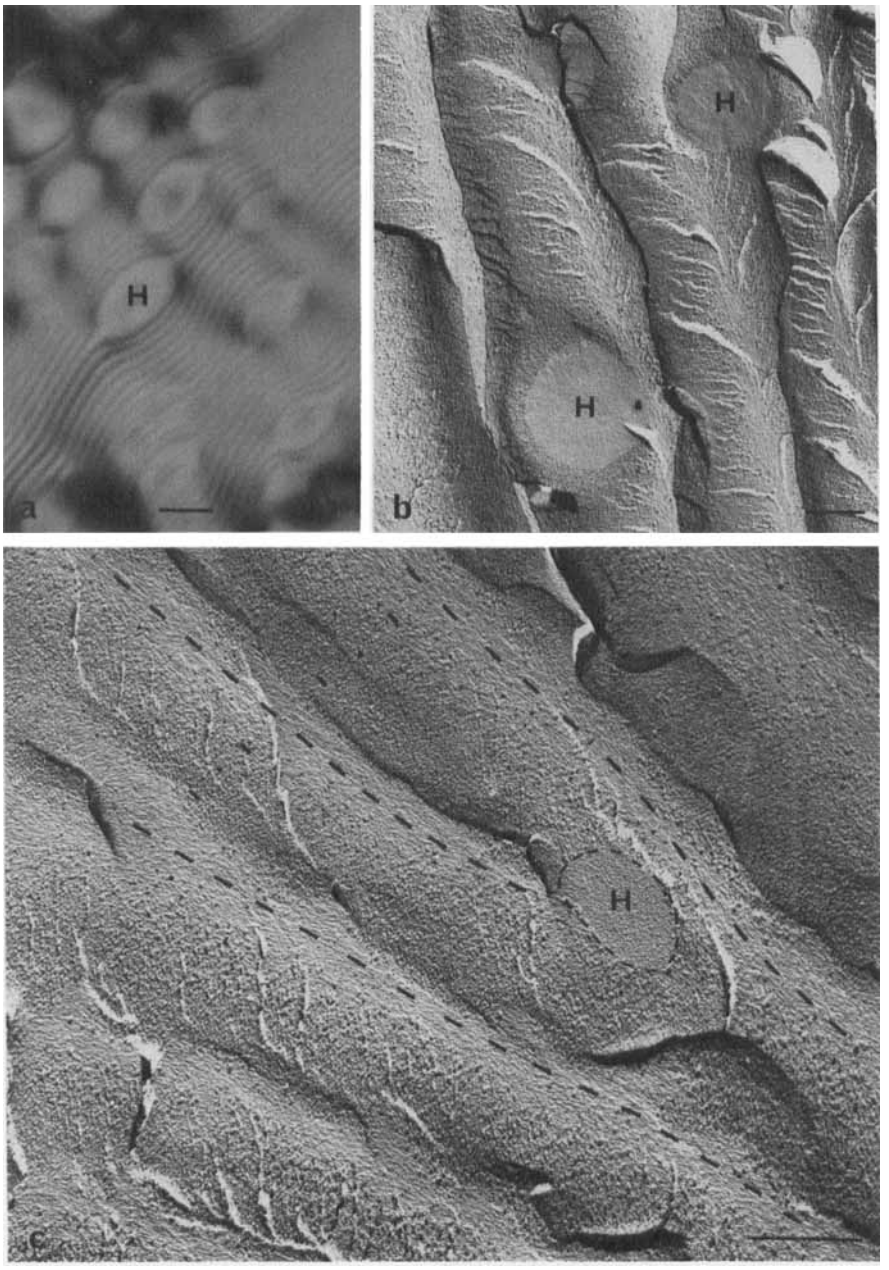

FIGURE 4 Phase transition between the cholesteric and the hexagonal phase. **a** : Germs of the hexagonal phase (H) growing within the cholesteric one (observation in polarizing microscopy ; bar = 10 μm). **b** : The resolution of the electron microscopy permits us to observe the first germs of the hexagonal phase (H). They appear as higher density areas within the cholesteric stratification (bar = 1 μm). **c** : Hexagonal germ located in the core of a $\lambda^{-}\tau^{+}$ edge dislocation. Molecular orientations are underlined to facilitate the observation (bar = 1 μm).

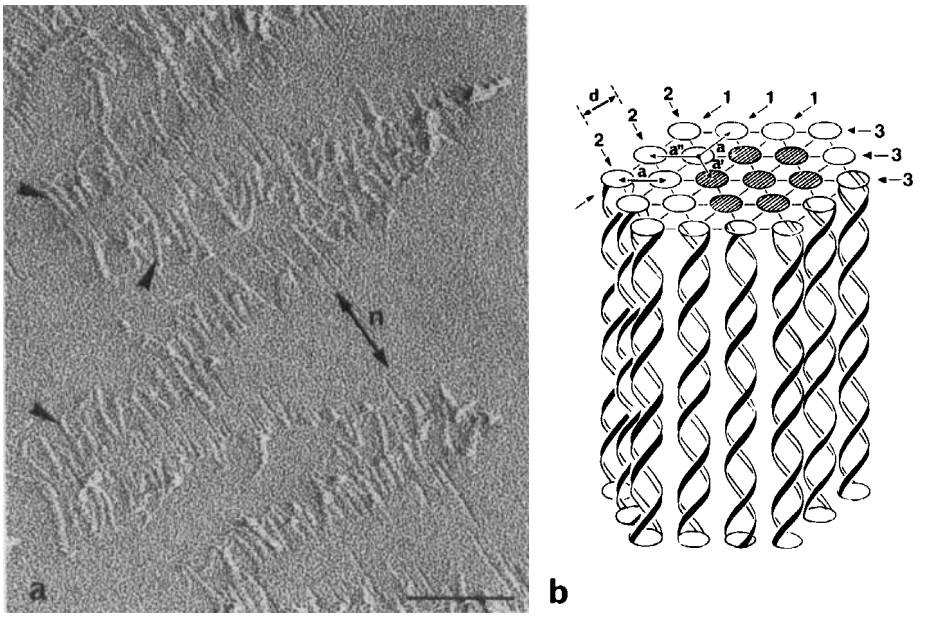

FIGURE 5 Columnar hexagonal phase. **a** : Layer of DNA molecules observed in electron microscopy after freeze-fracture. Molecules are aligned in parallel along a direction **n** and they can be seen individually at the edge of the layer (►) (bar = 0.1 μm). **b** : Hexagonal packing of the DNA molecules in this phase with the three series of molecular layers (1, 2, 3), which are preferentially followed by the fracture plane (d = thickness of one layer ; a = interhelix spacing).

can be seen in polarizing microscopy (Fig. 6c) and in electron microscopy (Fig. 6d).The columns of molecules are now folded and there is formation of walls of discontinuity. A precise analysis of such micrographs indicates that the folding of the layers can occur either parallel or normal to the molecular orientation (Livolant *et al*, in preparation).

Liquid crystals and chromatin

Condensed chromatin can present the same geometry than DNA molecules in liquid crystals.

The cholesteric organization can be easily recognized in cell nuclei by the presence of series of nested arches when thin sections of the material are observed in electron microscopy. As interpreted by Bouligand [20], these series of arches are not real arches but they originate from the cholesteric organization (as explained in Fig.3). Such series of arches can be observed in bacterial nucleoids [21], in special kinds of mitochondria [22] and the best example is found in Dinoflagellate chromosomes [20,23]. A comparison between these chromosomes and the *in vitro* cholesteric phase of DNA reveals striking similarities[5]. The cholesteric germs and the chromosomes can be elongated, with the layers normal to their elongation axis. In both cases, the cholesteric organization was

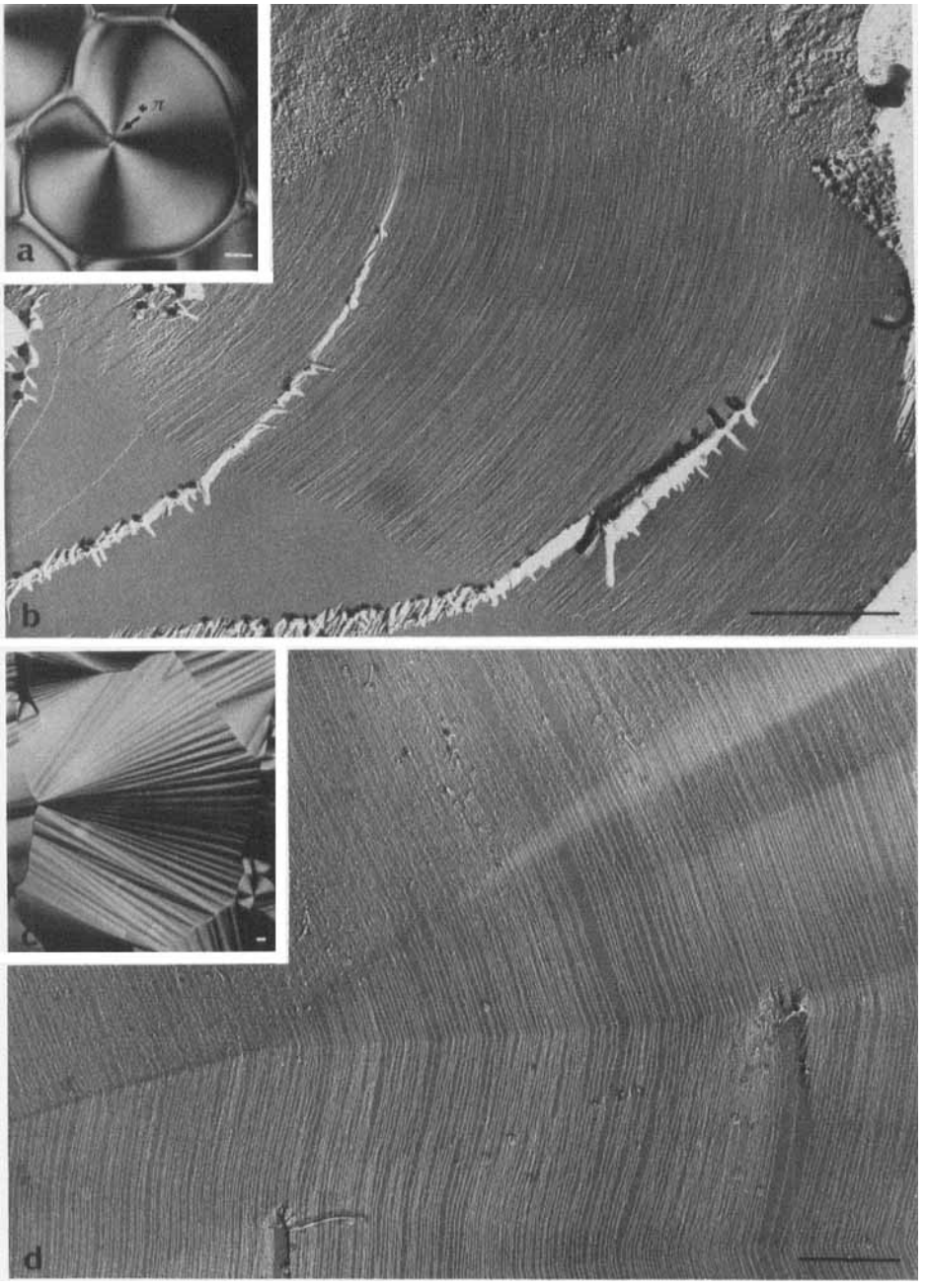

FIGURE 6 Evolution of the textures in polarizing (**a**, **c**) and electron (**b**, **d**) microscopy. **a**, **b** : Supple fan-shaped texture : the columns of molecules are coiled around a $+\pi$ disclination line. **c**, **d** : Striated fan-shaped texture : folding of the layers occuring when the DNA concentration is increased (bar = 10 μm in **a**, **c** ; 0.5 μm in **b**, **d**).

shown to be left-handed [24-25]. The same patterns are observed in electron microscopy for the different orientations of the fracture plane [17]. However, there are differences between the two systems, namely in the values of the helical pitch and in the nature of the defects. *In vitro*, the helical pitch is usually in the range of 2 to 3 μm, with much smaller values (0.2 to 0.4 μm) or much larger ones (up to 5 μm) when we are close to the transition to the more concentrated phase. In the cells, the helical pitch (P) ranges from 0.05 to 0.45 μm [26]. The smaller helical pitches are observed in sperm nuclei (0.05 to 0.07 μm, depending on the species). P varies from about 0.1 to 0.28 μm in bacteria, and from 0.07 to 0.45 μm in Dinoflagellate chromosomes. In these two cases, the helical pitch varies with the species but also within a given species with the physiological conditions. There are also differences in the nature of the defects observed *in vitro* and *in vivo*. Disclinations are exclusively of the λ type *in vitro* and of the τ type *in vivo*. The different kinds of dislocations can be found in both systems but the addition of successive layers (n times P/2) is preferred in chromosomes instead of the addition of several layers simultaneously (once nP/2) [5]. These differences are probably due to differences in the length of the DNA molecules and to the presence of other components in chromatin, namely RNA and proteins.

A hexagonal packing of DNA molecules can be found in some sperm nuclei (sepia, trout, salmon) [27,28] and in virus capsids [29].

Thus, it appears that condensed chromatin can present highly ordered structures, similar to those described in liquid crystalline phases of DNA [5,17,26]. Therefore, the liquid crystalline properties of DNA are probably involved in the process of condensation of chromatin *in vivo*. Methods of electron microscopy make now possible to compare these structures very accurately.

Acknowledgements : This research was supported by a grant from ARC.

REFERENCES

1. E. Kellenberger, E. Carlemalm, J. Sechaud, A. Ryter, G. de Haller, in *Bacterial Chromatin*, C. Gualerzi and C.L. Pon eds. (Springer Verlag, Berlin) 1986, p. 11.
2. C. Robinson, *Tetrahedron* **13**, 219-234 (1961).
3. L.S. Lerman, *Cold Spring Harb. Symp. Quant. Biol.* **38**, 59-73 (1974).
4. E. Senechal, G. Maret and K. Dransfeld, *Int. J. Biol. Macromol.* **2**, 256-262 (1980).
5. F. Livolant, *Eur. J. Cell Biol.* **33**, 300-311 (1984).
6. Y. Bouligand and F. Livolant, *J. Physique* **45**, 1899-1923 (1984).
7. F. Livolant, *J. Physique* **47**, 1605-1616 (1986).
8. F. Livolant and Y. Bouligand, *J. Physique* **47**, 1813-1827 (1986).
9. R.L. Rill, *Proc. ntl. Acad. Sci.* USA **83**, 342-346 (1986)
10. T.E. Strzelecka, M.W. Davidson and R.L. Rill, *Nature* **331**, 457-460 (1988).
11. Yu. M. Yevdokimov, S.G. Skuridin and V.J. Salyanov, *Liquid Crystals* **3**, 14431459 (1988).
12. F. Livolant, A.M. Levelut, J. Doucet and J.P. Benoit, *Nature* **339**, 724-726 (1989).
13. T.E. Strzelecka and R.L. Rill, *J. Amer. Chem. Soc.*, **109**, 4513-4518 (1987).
14. A. Leforestier, F. Livolant, *Biol. Cell* **71**, (1991), under press.

15. F. Livolant, *J. Physique* **48**, 1051-1066 (1987).
16. D.H. Van Winckle, M.W. Davidson, W.X. Chen and R.L. Rill, *Macromolecules* **23**, 4140-4148 (1990).
17. R.L. Rill, F. Livolant, H.C. Aldrich and M.W. Davidson, *Chromosoma* **98**, 280-286 (1989).
18. T.E. Strzelecka and R.L. Rill, *Biopolymers* **30**, 57-71 (1990).
19. F. Livolant, *J. Mol. Biol.* **218**, 165-181 (1991).
20. Y. Bouligand, M.O. Soyer, S. Puiseux-Dao, *Chromosoma* **24**, 251-287 (1968).
21. J.P. Gourret, *Biol. Cell.* **32**, 299-306 (1978).
22. G. Brugerolle and J.P. Mignot, *Biol. Cell* **35**, 111-114 (1979).
23. F. Livolant and Y. Bouligand, *Chromosoma* **68**, 21-44 (1978).
24. F. Livolant, M.M. Giraud and Y. Bouligand, *Biol. Cell.* **31**, 159-168 (1978).
25. F. Livolant and M.F. Maestre, *Biochemistry* **27**, 3056-3068 (1988).
26. F. Livolant, Workshop "*Ordering in Supramolecular Fluids*", Amsterdam, October 1990. *Physica A* (submitted).
27. M. Feughelman, R. Langridge, W.E. Seeds, A.R. Stokes, H.R. Wilson, M.H.F. Wilkins, R.K. Barclay and L.D. Hamilton, *Nature* **175**, 834-838 (1955).
28. V. Luzzati and A. Nicolaieff, *J. Mol. Biol.* **7**, 142-163 (1959).
29. J. Lepault, J. Dubochet, W. Baschong and E. Kellenberger, *EMBO J.* **6**, 1507-1512 (1987).